Inorg. Chem. **2005**, *44*, 7981–7991

Cubic and Spirocyclic Radicals Containing a Tetraimidophosphate Dianion $[P(NR)_3(NR')]^{\bullet 2-}$

Andrea F. Armstrong,[†] Tristram Chivers,*[,†] Heikki M. Tuononen,[†] Masood Parvez,[†] and René T. Boeré[‡]

Department of Chemistry, University of Calgary, Calgary, Alberta, Canada T2N 1N4, and Department of Chemistry and Biochemistry, University of Lethbridge, Lethbridge, Alberta, Canada T1K 3M4

Received July 7, 2005

The reaction of $Cl_3PNSiMe_3$ with 3 equiv of LiHNR (R = ^{i}Pr, Cy, ^{t}Bu, Ad) in diethyl ether produces the corresponding tris(amino)(imino)phosphoranes $(RNH)_3PNSiMe_3$ (**1a**, R = ^{i}Pr; **1b**, R = Cy; **1c**, R = ^{t}Bu; **1d**, R = Ad); subsequent reactions of **1b**–**d** with ^{n}BuLi yield the trilithiated tetraimidophosphates $\{Li_3[P(NR)_3(NSiMe_3)]\}$ (**2a**, R = Cy; **2b**, R = ^{t}Bu; **2c**, R = Ad). The reaction of $[(^t BuNH)_4P]Cl$ with 1 equiv of ^{n}BuLi results in the isolation of $(^t BuNH)_3PN^tBu$ (**1e**); treatment of **1e** with additional ^{n}BuLi generates the symmetrical tetraimidophosphate $\{Li_3[P(N^tBu)_4]\}$ (**2d**). Compounds **1** and **2** have been characterized by multinuclear (^{1}H, ^{13}C, and ^{31}P) NMR spectroscopy; X-ray structures of **1b**,**c** were also obtained. Oxidations of **2a**–**c** with iodine, bromine, or sulfuryl chloride produces transient radicals in the case of **2a** or stable radicals of the formula $\{Li_2[P(NR)_3(NSiMe_3)]LiX\cdot 3THF\}^\bullet$ (X = Cl, Br, I; R = ^{t}Bu, Ad). The stable radicals exhibit C_3 symmetry and are thought to exist in a cubic arrangement, with the monomeric LiX unit bonded to the neutral radical $\{Li_2[P(NR)_3(NSiMe_3)]\}^\bullet$ to complete the Li_3N_3PX cube. Reactions of solvent-separated ion pair $\{[Li(THF)_4]\{Li(THF)_2[(\mu\text{-}N^tBu)_2P(\mu\text{-}N^tBu)_2]Li(THF)_2\}$ (**6**) with I_2 or SO_2Cl_2 produce the persistent spirocyclic radical $\{(THF)_2Li(\mu\text{-}N^tBu)_2P(\mu\text{-}N^tBu)Li(THF)_2\}^\bullet$ (**10a**); all radicals have been characterized by a combination of variable concentration EPR experiments and DFT calculations.

Introduction

Investigations into the design and synthesis of persistent and stable[1a] inorganic radicals represent an active area of inorganic chemical research.[1b] Interest in stable radicals stems from their potential utility in several branches of chemistry, particularly as polymerization catalysts,[2] spin-labels for biomolecules,[3] and magnetic materials.[4] Though most radicals are transient species due to their open-shell electronic configurations, kinetic stabilization can be combined with delocalization of the unpaired electron over several electronegative atoms to produce stable or, at least, persistent radicals. Of especial interest at the present time are phosphorus-containing radicals,[5−11] as hyperfine coupling of the

* To whom correspondence should be addressed. E-mail: chivers@ucalgary.ca. Telephone: (403) 220-5741. Fax: (403) 289-9488.
[†] University of Calgary.
[‡] University of Lethbridge.

(1) (a) As defined in ref 1b, a "stable" radical is one which is inherently stable as an isolated species and does not decompose under an inert atmosphere at room temperature. A "persistent" radical is one which has a relatively long lifetime under the conditions which are used to generate it. (b) For a recent review, see: Power, P. *Chem. Rev.* **2003**, *103*, 789.
(2) See, for example: Hawker, C. *Acc. Chem. Res.* **1997**, *30*, 373.
(3) Turnbull, M. M.; Sugimoto, T.; Thompson, L. K. *Molecule-Based Magnetic Materials: Theory, Techniques, and Applications*; American Chemical Society: Washington, DC, 1996.
(4) Berliner, L. J. *Spin Labeling: Theory and Applications*; Academic Press: New York, 1979; Vol. 2.
(5) For a recent review, see: Armstrong, A.; Chivers, T.; Boeré, R. T. *Modern Aspects of Main Group Chemistry: The Diversity of the Stable and Persistent Phosphorus-Containing Radicals*; ACS Symposium Series; American Chemical Society: Washington, DC, 2005; Vol. 917, 66−80. Some recent examples of *neutral* P-containing radicals are reported in refs 6−11.
(6) Canac, Y.; Baceiredo, A.; Schoeller, W. W.; Gigmes, D.; Bertrand, G. *J. Am. Chem. Soc.* **1997**, *119*, 7579.
(7) Dumitrescu, A.; Rudzevich, V. L.; Romanenko, V. D.; Mari, A.; Schoeller, W.; Bourissou, D.; Bertrand, G. *Inorg. Chem.* **2004**, *43*, 6546.
(8) (a) Cataldo, L.; Dutan, C.; Misra, S. K.; Loss, S.; Grützmacher, H.; Geoffroy, M. *Chem.*—Eur. J. **2005**, *11*, 3463 (b) Loss, S.; Magistrato, A.; Cataldo, L.; Hoffmann, S.; Geoffroy, M.; Rothlisberger, U.; Grützmacher, H. *Angew. Chem., Int. Ed.* **2001**, *40*, 723.
(9) Hinchley, S. L.; Morrison, C. A.; Rankin, D. W. H.; Macdonald, C. L. B.; Wiacek, R. J.; Voigt, A.; Cowley, A. H.; Lappert, M. F.; Gundersen, G.; Clyburne, J. A. C.; Power, P. P. *J. Am. Chem. Soc.* **2001**, *123*, 9045.
(10) Bezombes, J. P.; Borisenko, K. B.; Hitchcock, P. B.; Lappert, M. F.; Nycz, J. E.; Rankin, D. W. H.; Robertson, H. E. *Dalton. Trans.* **2004**, 1980.
(11) For a review of P-containing verdazyl radicals, see: Hicks, R. G. *Can. J. Chem.* **2004**, *82*, 1119.

10.1021/ic051128q CCC: $30.25
Published on Web 10/11/2005

unpaired electron to the ^{31}P ($I = {}^1/_2$, 100%) nucleus results in much larger hyperfine coupling constants (HFCCs) than those observed for other abundant spin-active nuclei such as ^{14}N ($I = 1$, 99%) due to the larger gyromagnetic ratio of phosphorus (^{31}P, $\gamma = 10.83 \times 10^7$ rad/(T·s); ^{14}N, $\gamma = 1.933 \times 10^7$ rad/(T·s)).[12] From a fundamental standpoint, stable radicals are intriguing as they exist in violation of one of the fundamental tenets of chemical bonding theory—that electrons are usually paired in molecular compounds of the p-block elements.

Previously we reported that the reaction of $(^tBuNH)_3PNSiMe_3$ (**1c**) with *n*-butyllithium yields the dimeric trilithiated tetraimidophosphate $\{Li_3[P(N^tBu)_3(NSiMe_3)]\}_2$ (**2b**), which exists as a bicapped Li_6N_6 hexagonal prism.[13] The one-electron oxidation of **2b** with bromine or iodine has resulted in the isolation of the stable neutral radicals $\{Li_2[P(N^tBu)_3(NSiMe_3)]LiX{\cdot}3THF\}^\bullet$ (**3b**, X = Br; **3c**, X = I); the solution EPR characterization of these radicals and the X-ray structure of **3c** were reported in a preliminary communication.[14] In the solid state, the dilithiated tetraimidophosphate radical $\{Li_2[P(N^tBu)_3(NSiMe_3)]\}^\bullet$ was observed to trap a monomeric LiX unit, forming the distorted PN_3Li_3X cube **3b** or **3c**. The $NSiMe_3$ group is *exo* to the cluster, and a molecule of THF is coordinated to each lithium cation. We have also shown that this neutral radical can trap a monomeric lithium alkoxide, specifically LiO^tBu, forming the cluster $\{Li_2[P(N^tBu)_3(NSiMe_3)]LiO^tBu{\cdot}3THF\}^\bullet$ (**3d**), which is isostructural with **3b**,**c**.[15]

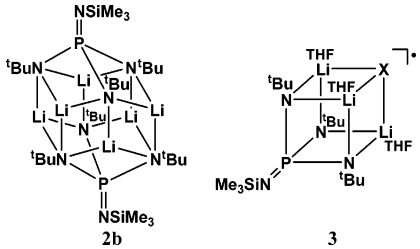

2b **3**

Although several persistent and stable neutral phosphorus-containing radicals are known,[5−11] only the 1,3-diphosphaallyl, $[^iPr_2NPC(N^iPr_2)PN^iPr_2]^\bullet$,[6] and tetraimidophosphate radicals **3b**−**d** are stable in the solid state and only **3c**,**d** have been characterized by X-ray crystallography.[14,15] The remarkable stability of these radicals can be attributed to the delocalization of spin density over two or four nitrogen atoms, respectively, as well as the presence of bulky isopropyl or *tert*-butyl substituents to impede their reactivities.

Initial studies[14] of **3b**,**c** indicated that the EPR spectra of these two radicals are dependent on both temperature and sample concentration. At extreme dilution, distortions in the EPR spectrum of **3b** had been suggested to result from disruption of the cubic framework to form a monocyclic radical; alternatively, it is conceivable that a mixture of paramagnetic species is present in solution. More recently, we have reported the synthesis and EPR characterization of the persistent spirocyclic radicals[16] $\{Me_2Al[(\mu\text{-}NR)(\mu\text{-}N^tBu)P(\mu\text{-}N^tBu)_2]Li(THF)_2\}^\bullet$ (**4a**, R = $SiMe_3$; **4b**, R = ^{t}Bu) in which the tetraimidophosphate ligand bis-chelates one lithium cation and one dimethylaluminum cation. These species were found to be considerably less stable than the cubic radicals **3**.

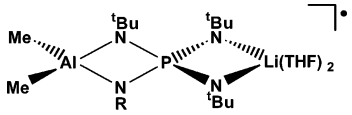

4

To gain further insight into the sources of stability of tetraimidophosphate radicals, a series of mixed amino/imino compounds $(RNH)_3PNSiMe_3$ (**1a**, R = ^{i}Pr; **1b,** R = Cy; **1c**, R = ^{t}Bu; **1d**, R = Ad) and $(^tBuNH)_3PN^tBu$ (**1e**) have now been synthesized and characterized; the reactions of their trilithium salts $\{Li_3[P(NR)_3(NSiMe_3)]\}_x$ (**2a**, R = Cy, **2b**, R = ^{t}Bu; **2c**, R = Ad) and $\{Li_3[P(N^tBu)_4]\}$ (**2d**) with oxidizing agents are described below. The radicals so produced have been characterized by a combination of variable concentration EPR spectroscopy and theoretical calculations.

Experimental Section

Reagents and General Procedures. All experiments were carried out under an argon atmosphere using standard Schlenk techniques. Tetrahydrofuran (THF) and *n*-hexane were dried over Na/benzophenone, distilled, and stored over molecular sieves prior to use. Bromine and ^{n}BuLi (2.5 M solution in hexanes) were used as received from Aldrich. The lithium amides LiHNR (R = Cy, Ad) were prepared by the reaction of the corresponding primary amines with ^{n}BuLi. Iodine was sublimed prior to use. $Cl_3PNSiMe_3$ [17] and $[(^tBuNH)_4P]Cl$[18] were prepared according to the literature procedures; $Cl_3PNSiMe_3$ was freshly distilled prior to use.

Instrumentation. ^1H, ^{13}C, ^7Li, and ^{31}P NMR spectra were collected on a Bruker DRX-400 spectrometer at 22 °C. The ^7Li and ^{31}P chemical shifts are reported relative to 1.0 M LiCl in D_2O and 85% H_3PO_4 in D_2O, respectively, while the ^1H and ^{13}C spectra were referenced internally to ^1H impurities in the deuterated solvents. Infrared spectra were recorded as Nujol mulls on KBr plates using a Nicolet Nexus 470 FTIR spectrometer in the range 4000−400 cm^{-1}. EPR spectra were recorded on a Bruker EMX 113 spectrometer; all spectra were recorded at 22 °C, unless otherwise noted. Spectral simulations were carried out using XEMR[19] and WINEPR SimFonia;[20] hyperfine coupling constants and line widths used to create spectral simulations are summarized in Table 4. Lorentzian line shapes were used in all simulations. The *g*-values of the radicals were calculated using the field/

(12) Weil, J. A.; Bolton, J. R.; Wertz, J. E. *Electron Paramagnetic Resonance: Elementary Theory and Practical Applications*; Wiley-Interscience: New York, 1994.
(13) Armstrong, A.; Chivers, T.; Krahn, M.; Parvez, M.; Schatte, G. *Chem. Commun.* **2002**, 2332.
(14) Armstrong, A.; Chivers, T.; Parvez, M.; Boeré, R. T. *Angew. Chem., Int. Ed.* **2004**, *43*, 502.
(15) Armstrong, A.; Chivers, T.; Parvez, M.; Schatte, G.; Boeré, R. T. *Inorg. Chem.* **2004**, *43*, 3453.
(16) Armstrong, A. F.; Chivers, T.; Tuononen, H. M.; Parvez, M. *Inorg. Chem.* **2005**, *44*, 5778.
(17) Wang, B.; Rivard, E.; Manners, *Inorg. Chem.* **2002**, *41*, 1690.
(18) Cameron, T. B.; Hanson, H. N.; de la Fuente, G. F.; Huheey, J. E. *Phosphorus, Sulfur, Silicon.* **1993**, *78*, 37.
(19) Eloranta, J. *XEMR*, version 0.7; University of Jyväskylä: Jyväskylä, Finland.
(20) *WINEPR SimFonia*, version 1.25; Bruker Analytische Messtechnik GmbH: 1996.

frequency ratio of each sample. Elemental analyses were provided by the Analytical Services Laboratory, Department of Chemistry, University of Calgary.

Synthesis of (^{i}PrNH)$_3$PNSiMe$_3$ (1a). $Cl_3PNSiMe_3$ (3.011 g, 13.41 mmol) was added slowly to a white slurry of LiHN^{i}Pr (2.617 g, 40.24 mmol) in diethyl ether (40 mL) at 22 °C producing a creamy suspension. After 4 h, the reaction mixture was filtered and the solvent was removed from the orange filtrate in vacuo leaving (^{i}PrNH)$_3$PNSiMe$_3$ as a yellow liquid (3.334 g, 11.40 mmol, 85%). ^{1}H NMR (C_6D_6, δ): 3.31 (m, C*H*Me$_2$, 3 H), 1.80 (s, NH, 3 H), 1.04 [d, CH*Me*$_2$, $^4J(^1H-^{31}P)$ = 6.5 Hz, 18 H], 0.23 (s, 9 H, SiMe$_3$). $^{13}C\{^1H\}$ NMR (C_6D_6, δ): 65.81 (s, *C*HMe$_2$), 26.62 [d, CH*Me*$_2$, $^3J(^{13}C-^{31}P)$ = 23.1 Hz], 4.48 [d, SiMe$_3$, $^3J(^{13}C-^{31}P)$ = 14.9 Hz]. $^{31}P\{^1H\}$ NMR (C_6D_6, δ): 7.1 (br, s). IR (neat): 3407.4 cm^{-1} (ν_{N-H}). Anal. Calcd for $C_{12}H_{33}N_4PSi$: C, 49.28; H, 11.37; N, 19.16. Found: C, 49.09; H, 11.70; N, 18.57.

Preparation of (CyNH)$_3$PNSiMe$_3$ (1b). A clear colorless solution of $Cl_3PNSiMe_3$ (2.983 g, 13.29 mmol) in diethyl ether (10 mL) was added to a white slurry of LiHNCy (4.189 g, 39.85 mmol) in diethyl ether (40 mL) at 0 °C producing a white slurry. After 2 h, the reaction mixture was warmed to 22 °C and stirred for an additional 14 h. The reaction mixture was filtered, and the solvent was removed in vacuo; the product was washed with pentane (10 mL) at −60 °C leaving (CyNH)$_3$PNSiMe$_3$ as a pale yellow solid (4.658 g, 11.29 mmol, 85%). ^{1}H NMR (C_6D_6, δ): 3.08 (m, NH), 1.94 (m), 1.60 (m), 1.22 (m), 1.00 (m), 0.41 (s, SiMe$_3$, 9 H). $^{13}C\{^1H\}$ NMR (C_6D_6, δ): 50.41 (s, N−CH), 36.82 [d, $^3J(^{13}C-^{31}P)$ = 14.0 Hz], 26.04 (s, CH$_2$), 25.73 (s, CH$_2$), 4.65 (s, SiMe$_3$). $^{31}P\{^1H\}$ NMR (C_6D_6, δ): 1.7 (s). IR (Nujol): 3408.6 (br), 3300.2 (s) cm^{-1} (ν_{N-H}). Anal. Calcd for $C_{33}H_{57}N_4PSi$: C, 61.12; H, 10.99; N, 13.58. Found: C, 59.66; H, 11.25; N, 13.46.

Preparation of (AdNH)$_3$PNSiMe$_3$ (1d). A clear colorless solution of $Cl_3PNSiMe_3$ (0.943 g, 4.20 mmol) in diethyl ether was added to a white slurry of LiHNAd (1.829 g, 11.64 mmol) in diethyl ether (40 mL) at 0 °C producing a pale blue slurry. After 1 h, the reaction mixture was warmed to 22 °C and stirred for an additional 18 h, resulting in a white slurry. The reaction mixture was filtered, and the solvent was removed in vacuo leaving (AdNH)$_3$PNSiMe$_3$ as a white powder (1.597 g, 2.81 mmol, 72%). ^{1}H NMR (C_6D_6, δ): 1.99 (br, 24 H, CH$_2$), 1.63 (br, 24 H, CH$_2$), 0.48 (s, 9 H, SiMe$_3$). $^{13}C\{^1H\}$ NMR (C_6D_6, δ): 51.24 [d, α-C, $^2J(^{13}C-^{31}P)$ = 5.1 Hz], 45.50 [d, NC(*C*H$_2$)$_3$, $^3J(^{13}C-^{31}P)$ = 17.1 Hz], 36.82 (s, CH), 30.36 (s, CH$_2$), 4.70 [d, SiMe$_3$, $^2J(^{13}C-^{31}P)$ = 9.6 Hz]. $^{31}P\{^1H\}$ NMR (C_6D_6, δ): −19.3 (s). Anal. Calcd for $C_{33}H_{57}N_4PSi$: C, 69.67; H, 10.10; N, 9.85. Found: C, 69.61; H, 10.27; N, 9.36.

Preparation of (^{t}BuNH)$_3$PN^{t}Bu (1e). A solution of ^{n}BuLi in hexane (0.92 mL, 2.3 mmol) was added to a white slurry of (^{t}BuNH)$_4$PCl (0.809 g, 2.28 mmol) in diethyl ether (20 mL) at 22 °C. The reaction mixture was stirred for 4 h and then filtered yielding a clear colorless solution. The solvent was removed in vacuo, leaving (^{t}BuNH)$_3$PN^{t}Bu as a white powder (0.541 g, 1.70 mmol, 75%). ^{1}H NMR (C_6D_6, δ): 1.52 (s, 9 H, ^{t}Bu), 1.29 (s, 27 H, ^{t}Bu). $^{13}C\{^1H\}$ NMR (C_6D_6, δ): 50.46 (s, N*C*Me$_3$), 50.42 (s, NH*C*Me$_3$), 35.45 [d, NCMe$_3$, $^2J(^{13}C-^{31}P)$ = 47.2 Hz], 32.13 [d, NHCMe$_3$, $^2J(^{13}C-^{31}P)$ = 16.7 Hz]. $^{31}P\{^1H\}$ NMR (C_6D_6, δ): −26.9 (s). Anal. Calcd for $C_{16}H_{39}N_4P$: C, 60.32; H, 12.35; N, 17.59. Found: C, 60.72; H, 12.50; N, 17.70.

Preparation of {Li$_3$[P(NCy)$_3$(NSiMe$_3$)]}$_2$ (2a). A solution of ^{n}BuLi in hexanes (8.75 mL, 14.0 mmol) was added to a clear pale yellow solution of (CyNH)$_3$PNSiMe$_3$ (1.925 g, 4.66 mmol) in hexane (25 mL) at 22 °C resulting in an off-white slurry. The reaction mixture was stirred for 4 h; the solvent was then removed in vacuo and the product washed with 3 × 5 mL of hexane. {Li$_3$[P(NCy)$_3$(NSiMe$_3$)]}$_2$ was recovered as a pale yellow powder (1.855 g, 2.155 mmol, 92%). ^{1}H NMR (THF-d_8, δ): 1.89 (m, CH), 1.63 (m, CH$_2$), 1.27 (m, CH$_2$), 1.05 (m, CH$_2$), 0.00 (s, SiMe$_3$). ^{7}Li NMR (THF-d_8, δ): −1.0−3.0 (br). $^{13}C\{^1H\}$ NMR (THF-d_8, δ): 53.97 (s, N*C*), 42.80 (s, CH$_2$), 27.62 (br, CH$_2$, CH$_2$), 6.42 (s, SiMe$_3$). $^{31}P\{^1H\}$ NMR (THF-d_8, δ): 36.1 (s). Anal. Calcd for $C_{21}H_{42}N_4PSi$: C, 58.59; H, 9.83; N, 13.02. Found: C, 57.50; H, 9.88; N, 11.87.

Preparation of {Li$_3$[P(NAd)$_3$(NSiMe$_3$)]}$_2$ (2c). A solution of ^{n}BuLi in hexanes (1.70 mL, 2.72 mmol) was added to an opaque mixture of (AdNH)$_3$PNSiMe$_3$ (0.510 g, 0.896 mmol) in hexane (20 mL) at 22 °C, resulting in an off-white slurry. The reaction mixture was stirred for 4 h; the solvent was then removed in vacuo leaving {Li$_3$[P(NAd)$_3$(NSiMe$_3$)]}$_2$ as a pale yellow solid (0.431 g, 0.367 mmol, 82%). ^{1}H NMR (THF-d_8, δ): (br, 24 H, CH$_2$), (br, 24 H, CH$_2$), (s, 9 H, SiMe$_3$). $^{13}C\{^1H\}$ NMR (THF-d_8, δ): 53.85 (s, N*C*), 50.08 [s, NC(*C*H$_2$)$_3$], 38.64 (s), 38.64 (s, CH), 32.27 (s, CH$_2$), 6.60 (s, SiMe$_3$). $^{31}P\{^1H\}$ NMR (THF-d_8, δ): 16.5 (br). Anal. Calcd for $C_{33}H_{54}N_4PSiLi_3$: C, 67.53; H, 9.28; N, 9.55. Found: C, 67.17; H, 10.40; N, 8.54.

Preparation of {Li$_3$[P(^{t}Bu)$_4$]} (2d). A solution of ^{n}BuLi in hexane (1.8 mL, 4.5 mmol) was added to a clear colorless solution of (^{t}BuNH)$_3$PN^{t}Bu (0.467 g, 1.466 mmol) in hexane (20 mL), resulting in a white slurry. The reaction mixture was stirred at 22 °C for 1 h; the solvent was then removed in vacuo, leaving {Li$_3$[P(N^{t}Bu)$_4$]} as a white powder (0.490 g, 1.457 mmol, 99%). ^{1}H NMR (THF-d_8, δ): 1.30 (s, ^{t}Bu). ^{7}Li NMR (THF-d_8, δ): 1.68, 0.93 (∼2:1). $^{13}C\{^1H\}$ NMR (THF-d_8, δ): 52.46 (s, *C*Me$_3$), 37.89 [d, C*Me*$_3$, $^2J(^{13}C-^{31}P)$ = 31.1 Hz]. $^{31}P\{^1H\}$ NMR (THF-d_8, δ): 7.4 (s). Satisfactory analyses could not be obtained due to the extremely hygroscopic nature of this sample.

Preparation of {Li$_2$[P(N^{t}Bu)$_3$(NSiMe$_3$)]LiCl·3THF}$^{\bullet}$ (3a). A solution of SO_2Cl_2 in hexane (1.33 mL, 0.332 mmol) was added to a clear colorless solution of {Li$_3$[P(N^{t}Bu)$_3$(NSiMe$_3$)]}$_2$ (0.234 g, 0.332 mmol) in THF/hexane (5 mL/15 mL) at 22 °C, resulting in a deep blue solution. After 5 min, the solvents were removed in vacuo leaving {Li$_2$[P(N^{t}Bu)$_3$(NSiMe$_3$)]LiCl·3THF}$^{\bullet}$ as a deep blue powder (0.213 g, 0.353 mmol, 53%).

Preparation of {Li$_2$[P(NAd)$_3$(NSiMe$_3$)]LiCl·3THF}$^{\bullet}$ (9a). A solution of SO_2Cl_2 in THF (1.54 mL, 0.154 mmol) was added to a pale yellow solution of {Li$_3$[P(NAd)$_3$(NSiMe$_3$)]}$_2$ (0.180 g, 0.153 mmol) in THF (15 mL) at 22 °C, resulting in a deep blue solution. After 5 min, the solvent was removed in vacuo leaving {Li$_2$[P(NAd)$_3$(NSiMe$_3$)]LiCl·3THF}$^{\bullet}$ as a deep blue powder (0.141 g, 0.168 mmol, 55%).

Preparation of {Li$_2$[P(NAd)$_3$(NSiMe$_3$)]LiI·3THF}$^{\bullet}$ (9b). A solution of I_2 in THF (10.0 mL, 1.02 mmol) was added to a pale yellow solution of {Li$_3$[P(NAd)$_3$(NSiMe$_3$)]}$_2$ (1.198 g, 1.021 mmol) in THF (20 mL) at 22 °C, resulting in a deep blue solution. After 15 min, the solvent was removed in vacuo and the product was extracted with 3 × 10 mL of hexane. Removal of the hexane in vacuo afforded {Li$_2$[P(NAd)$_3$(NSiMe$_3$)]LiI·3THF}$^{\bullet}$ as a deep blue powder (1.299 g, 1.397 mmol, 68%). Anal. Calcd for $C_{45}H_{78}N_4PSiILi_3O_3$: C, 58.12; H, 8.45; N, 6.02. Found: C, 56.84; H, 8.68; N, 6.23.

Oxidation of {Li$_3$[P(N^{t}Bu)$_4$]} (2d). A solution of I_2 in THF (4.4 mL, 0.19 mmol) was added to a pale yellow solution of Li$_3$[P(N^{t}Bu)$_4$] (0.129 g, 0.384 mmol) in THF (15 mL) at 22 °C, resulting in a gray-blue solution. After 72 h, the color had faded, leaving a yellow solution that was EPR silent.

A solution of SO_2Cl_2 in THF (2.5 mL, 0.25 mmol) was added to a pale yellow solution of Li$_3$[P(N^{t}Bu)$_4$] (0.167 g, 0.497 mmol) in THF (15 mL) at 22 °C, resulting in a green-blue solution. After

Table 1. Crystallographic Data

param	**1b**	**1c**
formula	$C_{21}H_{45}N_4PSi$	$C_{15}H_{39}N_4PSi$
fw	412.67	334.56
space group	$P2_1/n$	$R\bar{3}$
a, Å	10.5001(3)	14.7950(4)
b, Å	22.8914(7)	14.7950(4)
c, Å	20.9785(5)	16.3978(4)
α, deg	90	90
β, deg	101.7596(13)	90
γ, deg	90	120
V, Å^3	4936.6(2)	3108.46(14)
Z	8	6
T, K	173(2)	173(2)
λ, Å	0.710 73	0.710 73
d_{calcd}, g cm^{-3}	1.110	1.072
μ, mm^{-1}	0.173	0.19
F(000)	1824	1116
R^a	0.063	0.036
$R_w{}^b$	0.152	0.106

[a] $R = [\Sigma||F_o| - |F_c||]/[\Sigma|F_o|]$ for reflections with $I > 2.00\sigma(I)$. [b] $R_w = \{[\Sigma w(F_o^2 - F_c^2)^2]/[\Sigma w(F_o^2)^2]\}^{1/2}$ for all reflections.

42 h, the color had faded, leaving a yellow solution; no EPR signal was detected.

X-ray Analyses. Colorless crystals of **1b**,**c** were coated with Paratone 8277 oil and mounted on a glass fiber. All measurements were made on a Nonius Kappa CCD diffractometer using graphite-monochromated Mo Kα radiation. Crystallographic data are summarized in Table 1. The CCDC reference no. for **1c** is 190650. The structures were solved by direct methods[21] and refined by full matrix least-squares methods with SHELXL-97.[22] Hydrogen atoms were included at geometrically idealized positions and were not refined; the non-hydrogen atoms were refined anisotropically. Thermal ellipsoid plots were created using Diamond 2.1.[23]

Computational Details. The structures of the model radicals $\{Li_2[P(N^tBu)_3(NSiMe_3)]\cdot LiX\cdot 3OMe_2\}^\bullet$ (**5a**, X = Cl; **5b**, X = Br; **5c**, X = I; **5d**, X = O^{t}Bu) and $\{(Me_2O)_2Li(\mu\text{-}N^tBu)_2P(\mu\text{-}N^tBu)Li(OMe_2)_2\}^\bullet$ (**10b**) were optimized in their doublet ground states using density functional theory (DFT) and found to display near-C_3 (**5a**−**d**) and D_{2d} (**10b**) symmetry, respectively. Hybrid PBE0 exchange-correlation functional[24] and Ahlrichs' triple-ζ valence basis set augmented by one set of polarization functions (TZVP)[25] were used in the optimizations. All geometry optimizations were done with the Turbomole 5.7[26] program package.

Hyperfine coupling constants were calculated for all systems in their geometry- optimized structures using the unrestricted Kohn−Sham formalism. The nonrelativistic calculations utilized the same basis sets and density functional as the geometry optimizations; several benchmarks have recently been published which demonstrate the suitability of the TZVP basis set for the calculation of EPR parameters.[27] For the heavier nucleus iodine, the use of an effective core potential prevents the direct determination of the HFCC using the same method. In addition, relativistic calculations are essential to obtain more than a qualitative accuracy; thus, relativistic calculations were carried out for **5c**. The calculations utilized the large QZ4P STO basis set, the PBEPBE GGA[24a−c] functional as well as the scalar-relativistic ZORA formalism. The hyperfine coupling constant calculations were done with the Gaussian 03[28] (nonrelativistic) and ADF 2004.01[29] program packages (relativistic). The values reported are nonrelativistic for the lighter nuclei and scalar-relativistic for the heavier atom iodine.

Results and Discussion

Synthesis and NMR Characterization of 1a−d and X-ray structures of 1b,c. The tris(alkylamino)((trimethylsilyl)imino)phosphoranes $(RNH)_3PNSiMe_3$ (**1a**, R = ^{i}Pr; **1b**, R = Cy; **1c**, R = ^{t}Bu; **1d**, R = Ad) are readily obtained via the reaction of $Cl_3PNSiMe_3$ with 3 equiv of the corresponding lithiated amide LiHNR at room temperature in diethyl ether. The isopropyl derivative **1a** exists as a yellow oil at room temperature and has been characterized by ^{1}H and ^{31}P NMR spectroscopy. The ^{1}H NMR spectrum contains the expected two resonances which arise from the presence of three equivalent ^{i}Pr groups; an unresolved septet is observed at ~3.3 ppm due to the CH units, while the methyl groups produce a sharp doublet at 1.05 ppm. An additional resonance at 0.23 ppm is attributed to the trimethylsilyl fragment, and the relative integrations of these three resonances (3:18:9) confirm the identity of the product **1a**; a singlet is observed in the ^{31}P NMR spectrum at 7.1 ppm.

The heavier cyclohexyl analogue **1b** is a solid, which has been isolated in 85% yield. The ^{1}H NMR spectrum of **1b** consists of several broad multiplets due to unresolved ^{1}H−^{1}H couplings; the ^{13}C NMR spectrum, however, displays the four singlets characteristic of the cyclohexyl group, as well as a single resonance due to the $SiMe_3$ substituent. The ^{31}P NMR spectrum of **1b** contains the anticipated singlet at a chemical shift (1.7 ppm) that is similar to that observed for **1a**.

As reported previously,[13] the ^{1}H NMR spectrum of the *tert*-butyl derivative **1c** contains two peaks at 1.24 and 0.41

(21) Altomare, A.; Cascarano, M.; Giacovazzo, C.; Guagliardi, A. *J. Appl. Crystallogr*. **1993**, *26*, 343.

(22) Sheldrick, G. M. *SHELXL-97, Program for the Solution of Crystal Structures*; University of Göttingen: Göttingen, Germany, 1997.

(23) Brandenberg, K. *Diamond 2.1c*; Crystal Impact GbR: Bonn, Germany, 1999.

(24) (a) Perdew, J. P.; Burke, K.; Ernzerhof, M. *Phys. Rev. Lett.* **1996**, *77*, 3865. (b) Perdew, J. P.; Burke, K.; Ernzerhof, M. *Phys. Rev. Lett.* **1997**, *78*, 1396 (E). (c) Perdew, J. P.; Ernzerhof, M.; Burke, K. *J. Chem. Phys.* **1996**, *105*, 9982. (d) Ernzerhof, M.; Scuseria, G. E. *J. Chem. Phys.* **1999**, *110*, 5029.

(25) For iodine, an ECP basis set of triple-ζ valence quality was used. All basis sets were used as they are referenced in the Turbomole 5.7 internal basis set library.

(26) Ahlrichs, R.; et al. *TURBOMOLE, Program Package for ab initio Electronic Structure Calculations*, version 5.7; Theoretical Chemistry Group, University of Karlsruhe: Karlsruhe, Germany, 2004.

(27) (a) Hermosilla, L.; Calle, P.; Garcia de la Vega, J. M.; Sieiro, C. *J. Phys. Chem. A* **2005**, *109*, 1114. (b) Nguyen, M. T.; Creve, S.; Vanquickenborne, L. G. *J. Phys. Chem. A* **1997**, *101*, 3174. (c) Nguyen, M. T.; Creve, S.; Eriksson, L. A.; Vanquickenborne, L. G. *Mol. Phys.* **1997**, *91*, 537.

(28) Frisch, M. J.; Trucks, G. W.; Schlegel, H. B.; Scuseria, G. E.; Robb, M. A.; Cheeseman, J. R.; Montgomery, J. A., Jr.; Vreven, T.; Kudin, K. N.; Burant, J. C.; Millam, J. M.; Iyengar, S. S.; Tomasi, J.; Barone, V.; Mennucci, B.; Cossi, M.; Scalmani, G.; Rega, N.; Petersson, G. A.; Nakatsuji, H.; Hada, M.; Ehara, M.; Toyota, K.; Fukuda, R.; Hasegawa, J.; Ishida, M.; Nakajima, T.; Honda, Y.; Kitao, O.; Nakai, H.; Klene, M.; Li, X.; Knox, J. E.; Hratchian, H. P.; Cross, J. B.; Bakken, V.; Adamo, C.; Jaramillo, J.; Gomperts, R.; Stratmann, R. E.; Yazyev, O.; Austin, A. J.; Cammi, R.; Pomelli, C.; Ochterski, J. W.; Ayala, P. Y.; Morokuma, K.; Voth, G. A.; Salvador, P.; Dannenberg, J. J.; Zakrzewski, V. G.; Dapprich, S.; Daniels, A. D.; Strain, M. C.; Farkas, O.; Malick, D. K.; Rabuck, A. D.; Raghavachari, K.; Foresman, J. B.; Ortiz, J. V.; Cui, Q.; Baboul, A. G.; Clifford, S.; Cioslowski, J.; Stefanov, B. B.; Liu, G.; Liashenko, A.; Piskorz, P.; Komaromi, I.; Martin, R. L.; Fox, D. J.; Keith, T.; Al-Laham, M. A.; Peng, C. Y.; Nanayakkara, A.; Challacombe, M.; Gill, P. M. W.; Johnson, B.; Chen, W.; Wong, M. W.; Gonzalez, C.; Pople, J. A. *Gaussian 03*, revision C.02; Gaussian, Inc.: Wallingford, CT, 2004.

(29) *ADF2004.01*; SCM, Theoretical Chemistry, Vrije Universiteit: Amsterdam, The Netherlands, 2004; http://www.scm.com.

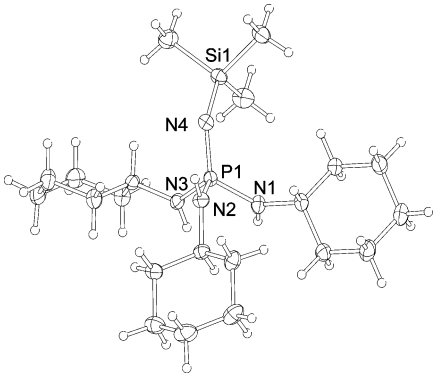

Figure 1. Thermal ellipsoid plot of **1b** (30% probability ellipsoids).

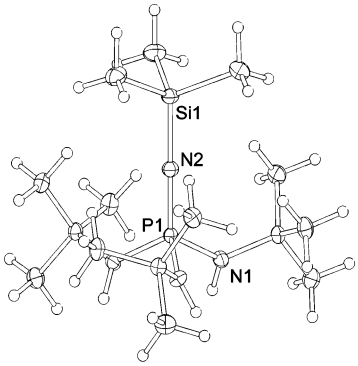

Figure 2. Thermal ellipsoid plot of **1c** (30% probability ellipsoids).

Table 2. Selected Bond Lengths (Å) and Angles (deg) for **1b**

P(1)−N(1)	1.648(2)	P(1)−N(3)	1.641(2)
P(1)−N(2)	1.646(3)	P(1)−N(4)	1.553(2)
Si(1)−N(4)	1.699(3)	N(2)−C(7)	1.466(4)
P(1)−N(1)−C(1)	122.9(2)	P(1)−N(2)−C(7)	127.3(2)
P(1)−N(3)−C(13)	125.1(2)	P(1)−N(4)−Si(1)	132.83(16)

ppm with integrations of 27 and 9 H assigned to the ^{t}Bu and $SiMe_3$ groups, respectively; the corresponding three resonances are observed in the ^{13}C NMR spectrum. A broad doublet, attributable to the NH protons, is also apparent in the ^{1}H NMR spectrum of **1c** at 1.92 ppm; no such resonance can be observed for **1b** due to overlap of the cyclohexyl signals in this region. However, the infrared spectra confirm the presence of NH units in **1a**−**c**, with sharp N−H stretching absorptions observed at 3409, 3407, and 3392 cm^{-1}. The ^{31}P NMR signal of **1c** appears at −13.6 ppm, i.e., at lower frequency than the resonances observed for **1a** (7.1 ppm) and **1b** (1.7 ppm), suggesting that the phosphorus nucleus of **1c** experiences significantly different shielding.

To probe the reason for this difference in ^{31}P NMR shifts, X-ray structures of both **1b**,**c** were obtained and are shown in Figures 1 and 2, respectively. In the solid state, the structure of **1b** displays four bent P−N−E (E = C, Si) linkages, with the three PNC bond angles averaging 125.1(2)°, and a slightly larger PNSi bond angle of 132.8(2)° (Table 2). As expected, the mean P−NHCy distance of 1.645(2) Å is substantially longer than the P═$NSiMe_3$ double bond length of 1.553(2) Å. In comparison, the P−NH^tBu bond length in **1c** is somewhat longer at 1.667(1) Å (Table 3), while the P═$NSiMe_3$ distance is less than that in **1b** at 1.520(2) Å. The most obvious and significant difference

Table 3. Selected Bond Lengths (Å) and Angles (deg) for **1c**[a]

P(1)−N(1)	1.520(2)	Si(1)−N(2)	1.667(2)
P(1)−N(2)	1.667(1)	N(1)−C(1)	1.485(2)
P(1)−N(1)−C(1)	127.19(9)	P(1)−N(2)−Si(1)	180.0

[a] Symmetry transformations used to generate equivalent atoms: (#1) $-y$, $x - y$, z; (#2) $-x + y$, $-x$, z.

between the structures of **1c** and **1b**, however, is that **1c** contains three bent P−N−C linkages [127.19(9)°] and a *linear* P−N−Si unit. This unexpected conformation is attributed to the influence of steric crowding caused by the three *tert*-butylamino groups and implies that the nitrogen lone pair on N(2) is not stereochemically active.

To examine this phenomenon in more detail, the model system H_3PNSiH_3 was analyzed at the PBE0 level of theory with the PNSi bond angle constrained at 180°. An electron localization function (ELF)-based bonding analysis did not reproduce a simple Lewis-type bonding arrangement, i.e., one monosynaptic nitrogen valence basin (lone pair) as well as two and one bisynaptic bonding basins for the PN and NSi units, respectively. Instead, the ELF analysis revealed a "superbasin" which is further split into mono- and bisynaptic valence basins. Rather than the "rabbit ear" type of lobe, which is characteristic of an sp^2 nitrogen atom, a torus-shaped ELF-basin was observed at the nitrogen atom, indicating that the lone pair is uniformly delocalized about the PNSi moiety to minimize the electron−electron repulsions involving the P−H bonds or, in the case of **1c**, the NH^tBu groups. This redistribution of electron density obviously has a large effect on the electronic environment at the phosphorus center, which is borne out in the observed differences between the ^{31}P NMR shifts of **1a**,**b** and **1c**. Similar steric effects are observed in derivatives of the trilithium salt of **1c**,[14,15] as well as in the sterically encumbered rhenium complex {$[(Me_3SiN)_2P(\mu\text{-}NSiMe_3)_2[\mu_3\text{-}Re(CO)_3]P(NSiMe_3)[N(SiMe_3)]_2$}in which the exocyclic $PNSiMe_3$ units display a nearly linear PNSi configuration [174(2)°].[30]

The adamantyl derivative **1d** is readily obtained in good yield (72%) via the reaction of $Cl_3PNSiMe_3$ with 3 equiv of LiHNAd at room temperature. The smaller yield of this product compared to those of **1a**,**b** is caused by the lower solubility of **1d** in diethyl ether, resulting in some product loss during filtration. Three broad resonances (1:2:2) are observed in the ^{1}H NMR spectrum of **1d** along with a sharp singlet due to the $SiMe_3$ group; better resolution is achieved in the ^{13}C spectrum which exhibits four sharp signals for the adamantyl units and a single resonance further upfield at 4.70 ppm, which is attributed to the trimethylsilyl substituent. The ^{31}P NMR signal of **1d** appears at −19.3 ppm, which is similar to the ^{31}P shift observed for **1c** (−13.6 ppm) but considerably upfield from those of **1a**,**b**, indicating that the electronic environment at the phosphorus center of **1d** is closer to that in **1c** than those in **1a** or **1b**. Although an X-ray structure of **1d** has not been obtained due to difficulties in growing suitable crystals, the ^{31}P NMR data suggest that

(30) Scherer, O. J.; Kerth, J.; Ziegler, M. L. *Angew. Chem., Int. Ed.* **1983**, *22*, 503.

the steric crowding from the bulky adamantyl groups results in a linear PNSi arrangement in **1d** as is observed for **1c** and its derivatives.[14,15]

To prepare a precursor to the symmetrical tetraimidophosphate $[P(NR)_4]^{3-}$ an alternative synthetic strategy was adopted using a variation on a literature procedure.[31] Rather than the reaction $[(^tBuNH)_4P]Cl$[18] with 4 equiv of ^{n}BuLi, which leads to the formation of tetraimidophosphates that are contaminated with various amounts of lithium chloride,[31] only 1 mol equiv of *n*-butyllithium was used. After removal of LiCl by filtration, the product $(^tBuNH)_3PN^tBu$ (**1e**) was recovered as a pure compound (eq 1) in good yield (75%). The ^{1}H NMR spectrum of **1e** displays two *tert*-butyl resonances at 1.52 and 1.29 ppm, with appropriate relative intensities, assigned to the imino and amino groups, respectively. The ^{13}C NMR spectrum also contains two sets of ^{t}Bu resonances, with signals at 50.46 and 33.45 ppm attributed to the N^{t}Bu group and resonances (50.42 and 32.13 ppm) assigned to the NH^{t}Bu units. A single resonance is observed in the ^{31}P spectrum at −26.9 ppm. Though this cannot be directly compared with the ^{31}P NMR signals for **1a**−**d** due to the different imino group present in **1e**, this upfield shift suggests considerable steric crowding at the phosphorus atom, which is consistent with the presence of four *tert*-butyl units.

$$[(^tBuNH)_4P]Cl + {}^nBuLi \xrightarrow[4\ h]{Et_2O} (^tBuNH)_3PN^tBu + LiCl \quad (1)$$

Synthesis and NMR Characterization of 2a−d. The unsymmetrical tetraimidophosphates $\{Li_3[P(NR)_3(NSiMe_3)]\}_2$ (**2a**, R = Cy; **2c**, R = Ad) can be prepared in much the same manner as the *tert*-butyl analogue $\{Li_3[P(N^tBu)_3(NSiMe_3)]\}_2$ (**2b**)[13] by the reaction of **1b** or **1d** with 3 equiv of *n*-butyllithium in organic solvents such as hexane or toluene at 22 °C. All attempts to prepare the isopropyl derivative "$\{Li_3[P(N^iPr)_3(NSiMe_3)]\}$" were unsuccessful, as 3-fold deprotonation could not be achieved regardless of the reaction conditions employed; only the $[P(N^iPr)_2(NH^iPr)(NSiMe_3)]^{2-}$ dianion was observed.

The cyclohexyl derivative **2a** is isolated in excellent yield (95%) after 4 h. Though the ^{1}H NMR spectrum of **2a** in THF-d_8 consists of a series of unresolved multiplets, the ^{13}C NMR spectrum shows the expected resonances due to the three equivalent cyclohexyl groups and an additional singlet attributed to the trimethylsilyl substituent. A single resonance at 36.1 ppm is observed in the ^{31}P NMR spectrum of **2a**, which is shifted significantly to higher frequency compared to the ^{31}P signal observed for **2b** (5.3 ppm).[13] This disparity is attributed to the different electronic environment at the phosphorus center due to the linear PNSi unit of **2b**,[13] as discussed earlier for **1b**,**c**. The ^{7}Li NMR spectrum of **2a** consists of a broad resonance spanning approximately 4 ppm, suggesting that the lithium cations are dynamic in THF solutions.

The adamantyl derivative **2c** was isolated in 72% yield. As was observed for **1d**, the ^{1}H NMR spectrum of **2c** is not well resolved, and the ^{13}C NMR spectrum gives a better indication of the identity of the product. Only four alkyl signals are observed, indicating the equivalence of the three adamantyl groups; an infrared spectrum showed no N−H stretching vibrations, confirming that **1d** has indeed been triply deprotonated. While an X-ray structure of **2c** could not be obtained due to difficulties in growing suitable crystals, the equivalence of the NAd units indicates that this molecule possesses C_3 symmetry and suggests that it may be isostructural with **2b**. The single resonance in the ^{31}P NMR spectrum (16.5 ppm) of **2b** confirmed its purity.

The symmetrical tetraimidophosphate $\{Li_3[P(N^tBu)_4]\}$ (**2d**) was prepared by trilithiation of the trisamino(imino)phosphorane **1e** with ^{n}BuLi. One resonance is observed at 7.4 ppm in the ^{31}P NMR spectrum of **2d** in THF-d_8, while the ^{1}H and ^{13}C NMR spectra indicate the existence of only one environment for the four *tert*-butyl groups. These spectroscopic data suggest that rather than displaying a dimeric hexagonal prism structure like **2a**−**c**, the tetraimidophosphate anion of **2d** adopts a spirocyclic conformation in solution due to partial solvation of its lithium cations by THF, to give the solvent-separated ion pair $\{[Li(THF)_4]\{Li(THF)_2[(\mu\text{-}N^tBu)_2P(\mu\text{-}N^tBu)_2]Li(THF)_2\}$ (**6**). The formation of a similar complex has been reported for the analogous naphthyl derivative $\{[Li(THF)_4][(THF)_2Li(\mu\text{-Nnaph})_2P(\mu\text{-Nnaph})_2Li(THF)_2]\}$ (**7**),[32] which is known to display a spirocyclic structure both in solution and in the solid state. This proposed geometry of **6** is corroborated by the ^{7}Li NMR spectrum of **2d** in THF-d_8, which contains signals at 1.68 and 0.93 ppm in an approximately 2:1 ratio that can be assigned to the N,N′-chelated lithium cations and the free $[Li(THF)_4]^+$ cation of the ion pair **6**, respectively.

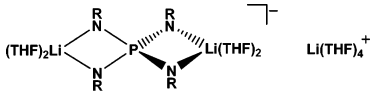

R = ^{t}Bu, **6**; R = naph, **7**

Variable Concentration EPR Studies of the Radicals $\{Li_2[P(N^tBu)_3(NSiMe_3)]LiX\cdot 3THF\}^\bullet$ (3a, X = Cl; 3b, X = Br; 3c, X = I). The oxidation of $\{Li_3[P(N^tBu)_3(NSiMe_3)]\}_2$ (**2b**) with 1 equiv of sulfuryl chloride in THF proceeds in much the same manner as the analogous reactions with iodine and bromine;[14] a deep blue-black solution forms immediately, indicating the presence of a radical species. Removal of the solvent in vacuo yields the stable neutral radical $\{Li_2[P(N^tBu)_3(NSiMe_3)]LiCl\cdot 3THF\}^\bullet$ (**3a**) as a bright blue solid. A finely powdered material is obtained by redissolving **3a** in hexane and decanting the deep blue solution, followed by immediate removal of the hexane in vacuo, as the stabilities of **3a**−**d** in hydrocarbon solvents are limited.

The structures of the distorted-cubic model radicals $\{Li_2[P(N^tBu)_3(NSiMe_3)]LiX\cdot 3OMe_2\}^\bullet$ (**5a**, X = Cl; **5b**,

(31) Bickley, J. F.; Copsey, M. C.; Jeffery, J. C.; Leedham, A. P.; Russell, C. A.; Stalke, D.; Steiner, A.; Stey, T.; Zacchini, S. *Dalton Trans.* **2004**, 989.

(32) Raithby, P. R.; Russell, C. A.; Steiner, A.; Wright, D. S. *Angew., Chem. Int. Ed.* **1997**, *36*, 649.

Table 4. HFCCs of the Tetraimidophosphate Radicals **3**, **5**, and **10** (G)

nuclei or param	**5a** calcd,[a] X = ^{35}Cl	**3a** in THF, X = ^{35}Cl	**3a** in hexane,[b] X = ^{35}Cl	**5b** calcd,[a] X = ^{79}Br	**5c** calcd,[a] X = ^{127}I	**3c** in THF,[b] X = ^{127}I	**3c** in hexane,[b] X = ^{127}I	**5d** calcd[a]	**3d** in THF[b]	**10b** calcd[a]	**10a** in THF[b]
^{31}P	−28.6	24.68	26.70	−28.4	−28.2	27.11	24.15	−29.3	25.19	−30.5	25.60
^{14}N	3.2	5.26	5.23	3.2	3.2	5.37	5.27	5.39	3.1	3.7	4.25
^{14}N	−0.6	0.40	0.51	−0.6	−0.6	0.20	0.40	0.36	−0.6	n/a	n/a
^{7}Li	−2.5	2.19	2.44	−2.6	−2.6	1.91	2.35	1.88	−2.3	−1.4	1.08
X	−0.2	0.10		−0.7	−0.8	0.53		n/a	n/a	n/a	n/a
line width[c]		0.60	1.20			0.50	0.40		0.32		0.40
g value		2.0051	2.0052			2.0053	2.0055		2.0048		2.005

[a] HFCCs calculated for the model systems **5a**−**d** and **10b**. [b] HFCCs used to create spectral simulations of **3a**, **3c**/**3d**, and **10a**. [c] Line widths used to create spectral simulations.

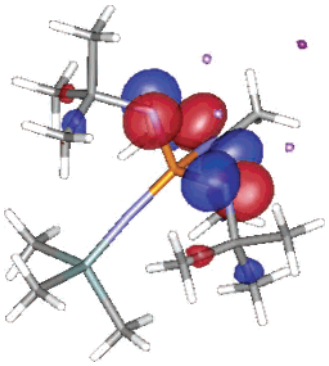

Figure 3. SOMO of **5c** with OMe_2 molecules omitted.

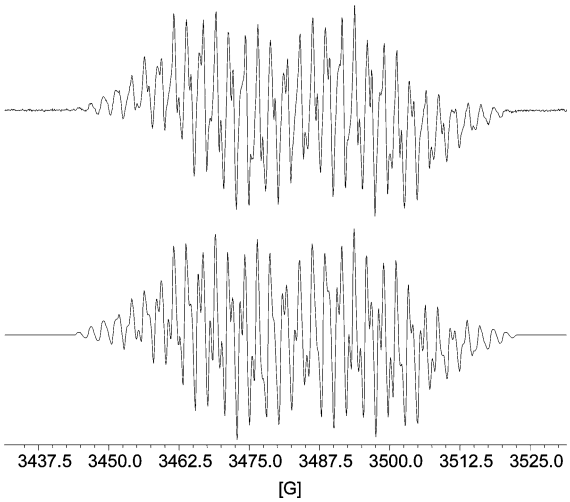

Figure 4. Experimental (top) and simulated (bottom) EPR spectra of **3a** (ca. 8 mM in THF).

X = Br; **5c**, X = I; **5d**, X = O^{t}Bu) were optimized and found to display near-C_3 symmetry. The calculated metrical parameters for **5c**,**d** are in good agreement (see Supporting Information) with the corresponding structural parameters of **3c**,**d**, respectively, which were determined by X-ray crystallography. The singly occupied molecular orbitals (SOMOs) of **5a**−**d** are essentially identical, with no dependence on the identity of the X atom or group observed. The SOMO of **5c**, as depicted in Figure 3, indicates that the spin density is primarily located in p-type orbitals on the three nitrogen atoms within the cubic framework. Consequently, the EPR spectra of these radicals are expected to exhibit large hyperfine couplings to three equivalent ^{14}N atoms, as well as a smaller coupling to the $NSiMe_3$ nitrogen atom. Though the SOMO indicates only minimal spin density on the phosphorus atom, a significant ^{31}P hyperfine coupling constant (HFCC) is anticipated due to a combination of spin-polarization effects and the large gyromagnetic ratio of that nucleus; similarly, couplings to three ^{7}Li cations and the halogen atom of **5a**−**c** are expected. The calculated HFCCs for these model systems are compiled in Table 4 along with the values used to create spectral simulations of **3a**,**c**,**d**. The similarities among the SOMOs of **5a**−**d** are reflected in their calculated HFCCs, of which only the halogen HFCC varies significantly from **5a** to **5c**. Thus, the differences among the appearances of the experimental EPR spectra of **3a**−**d** are attributed in large part to the identity (**3a**−**c**) or absence (**3d**) of the spin-active halogen atom.

EPR spectra of $\{Li_2[P(N^tBu)_3(NSiMe_3)]LiCl{\cdot}3THF\}^{\bullet}$ (**3a**) were recorded as a function of concentration in THF and hexane, but changes in the concentrations of the samples had no effect on the observed spectra. The EPR spectrum of **3a** in THF is shown in Figure 4. The main features of this spectrum can be reproduced by including hyperfine coupling constants (Table 4) to one phosphorus atom (a^{31}_P = 24.68 G), three equivalent lithium cations (^{7}Li, I = 3/2, 94%, a^{7}_{Li} = 2.19 G), and three equivalent nitrogen centers (a^{14}_N = 5.26 G). The additional fine structure is caused by a small coupling to the fourth and unique nitrogen atom (a^{14}_N = 0.40 G) and to the chlorine atom (a^{35}_{Cl} = 0.10 G).[33] The simulation created using these HFCCs and a line width of 0.6 G is shown in Figure 4 and is an excellent match with the experimental spectrum.

A comparison with the calculated HFCCs for the model system **5a** shows good agreement between the two sets of values, though the experimental ^{14}N^{t}Bu HFCCs are somewhat larger than the calculated values; conversely, the experimental ^{31}P HFCC is ca. 4 G smaller than expected. This systematic error has been observed previously in related studies.[16,34,35] It arises due to the apparent tendency of this functional basis set combination to underestimate couplings

(33) Though chlorine has two spin-active isotopes (^{35}Cl, 75.5%, I = 3/2; ^{37}Cl, 24.5%, I = 3/2), including hyperfine coupling to ^{37}Cl has no effect on the appearance of the simulation due to the low gyromagnetic ratio (γ-value) and natural abundance of that isotope; the ^{37}Cl HFCC of 0.08 G was determined by taking the ratio of the γ-values of the two isotopes and combining this with the optimum value of the ^{35}Cl HFCC. Thus, hyperfine coupling to ^{37}Cl is included in the spectral simulation for completeness but does not alter its appearance appreciably.

(34) Chivers, T.; Eisler, D. J.; Fedorchuk, C.; Schatte, G.; Tuononen, H. M.; Boeré, R. T. *Chem. Commun*. **2005**, 3930.
(35) Tuononen, H. M.; Armstrong, A. F. *Inorg. Chem.*, accepted for publication.

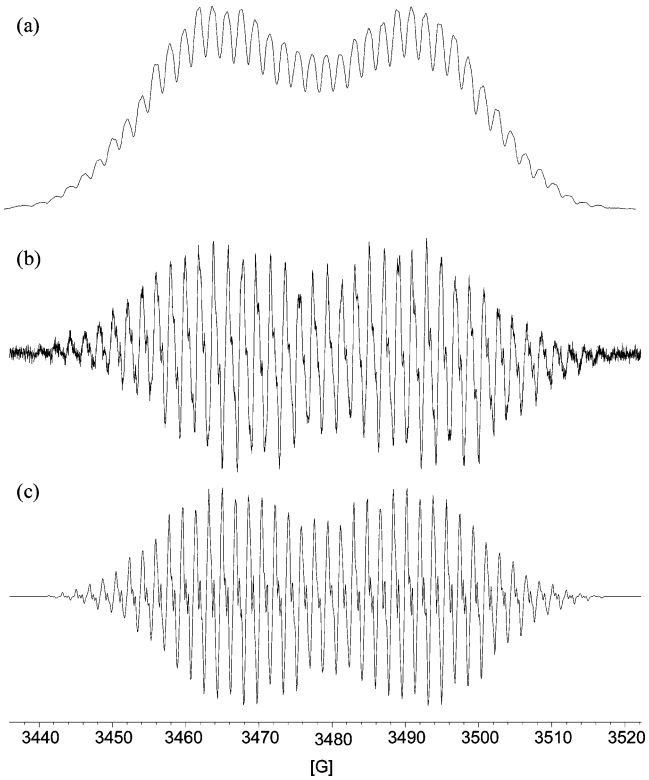

Figure 5. EPR spectra of **3d** in THF: (a) absorption mode; (b) dispersion mode; (c) simulation of cubic **3d**.

which result from the spin density of the unpaired electron, such as the $^{14}N^tBu$ couplings, while overestimating those which arise due to spin-polarization effects, as does the ^{31}P coupling. The EPR spectrum of **3a** in hexane (see Supporting Information) is consistent with the presence of a single cubic radical in solution and can be simulated by using HFCCs similar to those used to create the simulation of **3a** in THF. These HFCCs (Table 4) are in better agreement with those calculated for **5a** than are the HFCCs present in the spectrum of **3a** in THF. However, significant line-broadening is seen in this spectrum (lw $\approx$ 2 G) due to slower molecular tumbling of the polar cluster **3a** in the nonpolar solvent hexane, rendering the values of the HFCCs to the ^{35}Cl and $^{14}NSiMe_3$ atoms somewhat speculative.

The observation that the EPR spectrum of **3a** does not vary with sample concentration indicates that the cubic structure of this radical is retained even at extreme dilution in THF, in contrast to the earlier proposal for **3b**,**c**.[14] This finding prompted a reexamination of the EPR data reported previously for the lithium *tert*-butoxide adduct $\{Li_2[P(N^tBu)_3(NSiMe_3)](LiO^tBu)\cdot 3THF\}^\bullet$ (**3d**).[15] A good simulation of the EPR spectrum of this species had been obtained assuming dissociation of the cubic framework to yield the monocyclic radical $\{(THF)_2Li(\mu\text{-}N^tBu)(\mu\text{-}NSiMe_3)\text{-}P(N^tBu)_2]\}^{\bullet-}$; however, the fact that **3a** does not dissociate in solution would suggest that **3d** also retains its cubic structure, as the Li−X bonds which cement these frameworks are stronger for X = O than X = Cl. Inspection of the EPR spectrum of **3d** in the absorption mode (Figure 5) reveals an exponential decay pattern at both the high- and low-field ends of the resonance, which is characteristic of hyperfine coupling to more than one equivalent nucleus with $I > 1$, such as ^7Li. Integration of the spectral simulation published previously[15] does not reproduce this pattern. In consequence, the EPR spectrum of **3d** was simulated anew, assuming the C_3 symmetry which is expected for this cubic radical. By inclusion of HFCCs (Table 4) to one phosphorus atom (a_P = 25.19 G), three equivalent nitrogen atoms (a_N = 5.39 G), three equivalent lithium nuclei (a_{Li} = 1.88 G), and an additional ^{14}N coupling due to the *exo*-cluster $NSiMe_3$ group (a_N = 0.36 G), which accounts for the "jagged" appearance of the spectral lines, an excellent simulation of the experimental spectrum was obtained (Figure 5). Both the line spacings and intensities present in the spectrum in the dispersion mode and the decay pattern observed in the absorption spectrum are accurately reproduced by this new spectral simulation. In consequence, we consider that the simulation in Figure 5c is a more accurate representation of the EPR spectrum in Figure 5b than the simulation described previously.[15] The HFCCs that were used to create the new simulation (Table 4) are more accurate values for this radical, which, in the final analysis, appears to retain its cubic structure in dilute THF solutions.

In comparison to the EPR spectrum of **3a**, the EPR spectra obtained for the bromine analogue **3b** are considerably more complex. This additional hyperfine coupling arises in part due to the presence of a bromine atom which, like chlorine, has two spin-active isotopes. However, they are approximately equal in natural abundance (^{79}Br, I = 3/2, 50.7%; ^{81}Br, I = 3/2, 49.3%)[6] and have significantly larger gyromagnetic ratios, resulting in larger hyperfine coupling constants than those for the $^{35,37}Cl$ nuclei of **3a**. As the γ-values of ^{79}Br and ^{81}Br are quite similar, their HFCCs will differ only by a factor of 1.1, causing overlap between the spectral lines and further complicating the experimental spectrum.

Examination of a concentrated (ca. 8 mM) solution of **3b** in THF at 22 °C gives a strong indication that this radical also displays a cubic geometry, and while reasonable simulations can be constructed implementing a variety of different ^{14}N, ^7Li, and $^{79,81}Br$ HFCCs, no exact match with an experimental spectrum has been achieved. Though good approximations of the hyperfine coupling constants to ^{31}P and the three $^{14}N^tBu$ atoms can be extracted from the experimental spectrum, the plethora of fine structure due to the lithium cations, the fourth nitrogen atom, and the two bromine isotopes has rendered accurate determination of these HFCCs virtually impossible. However, conclusive evidence that **3b** exists as a cube at this concentration has been obtained previously in the form of a low-temperature EPR spectrum, which clearly indicated HFCCs to three equivalent ^{14}N atoms.[14]

The limiting EPR spectrum of **3b** in THF (ca. 1.5 mM), which was reported in a preliminary communication,[14] does not display the obvious inversion symmetry that is characteristic of a single paramagnetic species in solution and is observed in the EPR spectra of both **3a**,**d**. This spectral distortion, indicating the presence of a second paramagnetic species in solution, supports the hypothesis that, at extreme

Scheme 1. Dissociation of the Cubic Radicals **3b**,**c** to the Spirocycle **8** in Dilute THF Solutions (X = Br, I)

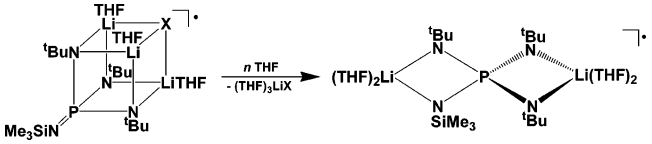

dilution in THF, partial dissociation of the cubic framework of **3b** occurs, presumably due to THF solvation of the lithium cations (Scheme 1). The expected products of this process are the neutral spirocyclic radical $\{(THF)_2Li[(\mu\text{-}N^tBu)(\mu\text{-}NSiMe_3)P(\mu\text{-}N^tBu)_2]Li(THF)_2\}^\bullet$ (**8**) in which two lithium cations are bis-chelated by the tetraimidophosphate ligand and a THF-solvated molecule of lithium bromide. The fact that this occurs for **3b** but not **3a** or **3d** can be attributed to the weaker nature of Li−Br bonds of **3b** as compared to the Li−X linkages present in **3a** (X = Cl) and **3d** (X = O).

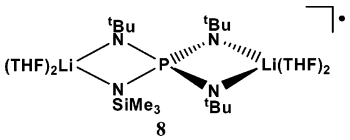

8

EPR spectra of the iodine-containing radical **3c** were also recorded as a function of concentration in both THF and hexane. The spectrum of a moderately concentrated sample (ca. 7 mM) in THF is shown in Figure 6 and exhibits a bimodal pattern like those of **3a**,**b**,**d** due to the presence of a large ^{31}P coupling. An excellent simulation of this spectrum was obtained by using HFCCs (Table 4) that are similar to those present in **3a** and a line width of 0.4 G; a significantly larger iodine HFCC ($a^{127}_I = 0.53$ G) is observed compared to the $^{35,37}Cl$ HFCC of **3a** due to the larger γ-value of the former isotope (^{127}I, $I = 5/2$, 100%, $\gamma = 5.35 \times 10^7$ rad/(T·s)). The difference in appearance between this EPR spectrum and that of **3a** in THF (Figure 3) can be attributed in large part to the presence of the higher spin nucleus ^{127}I. As was observed previously for **3a**,[14] the EPR spectrum of **3c** in hexane (see Supporting Information) is not dependent upon sample concentration, though significant line-broadening occurs (vide supra) even for extremely dilute solutions. This spectrum can be simulated accurately using HFCCs (Table 4) which are quite similar to those used to simulate the EPR spectrum of **3c** in THF, confirming that this radical retains its cubic structure in the noncoordinating solvent hexane.

The EPR spectrum of **3c** in THF is highly susceptible to concentration-dependent line-broadening. Dilution of the EPR sample to ca. 1.4 mM resulted in the acquisition of a limiting EPR spectrum (see Supporting Information), where nearly all the hyperfine couplings are resolved. A fairly accurate simulation of this spectrum is obtained using the same HFCCs as for the more concentrated sample but with a much smaller line width (0.2 G). The lack of an exact agreement between the experimental and simulated spectra may be indicative of the presence of a second paramagnetic species in solution as was observed for **3b**; however, the reasonable agreement observed indicates that the cubic radical is the predominant species at extreme dilution.

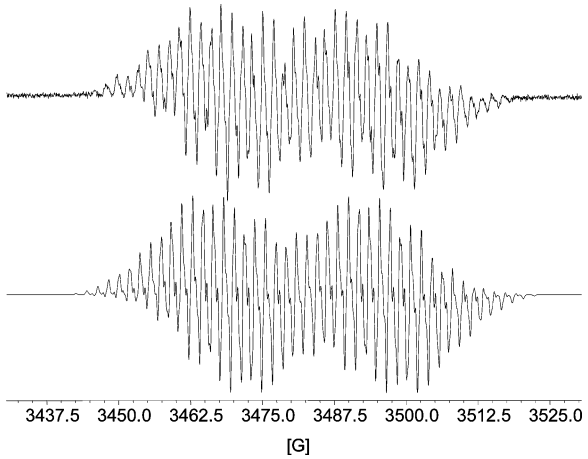

Figure 6. Experimental (top) and simulated (bottom) EPR spectra of **3c** (ca. 7.6 mM in THF).

At extremely low concentrations (<2 mM) in THF, the stability of **3c** is found to decrease significantly and the blue color of the solution fades appreciably over a period of a few hours. Concurrently, colorless crystalline needles are formed. An X-ray analysis has identified this material as $(THF)_3LiI$ indicating that, at extreme dilution, dissociation of the cubic framework of **3c** occurs with the extrusion of lithium iodide. If a second paramagnetic species is present in the EPR spectra of these extremely dilute THF solutions, it is thus thought to be the neutral spirocyclic radical $\{(THF)_2Li[(\mu\text{-}N^tBu)(\mu\text{-}NSiMe_3)P(\mu\text{-}N^tBu)_2]Li(THF)_2\}^\bullet$ (**8**), which is also believed to be present in dilute samples of **3b**. Attempts to identify and indeed confirm the presence of a second radical in solution by means of an electron nuclear double resonance (ENDOR) experiment were not successful.

Oxidation of 2a and 2c: Synthesis and EPR Characterization of the Stable Tetraimidophosphate Radicals $\{Li_2[P(NAd)_3(NSiMe_3)]LiX\cdot 3THF\}$ (9a, X = Cl; 9b, X = I). Reactions of $\{Li_3[P(NCy)_3(NSiMe_3)]\}_2$ (**2a**) with the oxidizing agents iodine or sulfuryl chloride SO_2Cl_2 produce blue solutions reminiscent of the tetraimidophosphate radicals described previously;[14−16] however, this color is fleeting, lasting for only a few seconds. Attempts to record EPR spectra of these transient radicals were unsuccessful as no signal could be observed due to the short lifetimes of these species. This pronounced decrease in stability upon replacing the *tert*-butyl groups of **2b** with cyclohexyl substituents of **2a** suggests that, without the kinetic stabilization provided by the steric bulk of the ^{t}Bu groups, the radicals either decompose or dimerize rapidly to a diamagnetic species.

In light of this observation, the effect of the replacement of the *tert*-butyl groups of the radicals **3** by even bulkier substituents was investigated. The oxidation of $\{Li_3[P(NAd)_3(NSiMe_3)]\}_2$ (**2c**) with iodine or sulfuryl chloride produces deep blue solutions; removal of the solvent in vacuo yields the paramagnetic blue powders $\{Li_2[P(NAd)_3(NSiMe_3)]LiX\cdot 3THF\}^\bullet$ (**9a**, X = Cl; **9b**, X = I), which are stable for long periods in the solid state. The EPR spectra of these two radicals are essentially identical, displaying a bimodal pattern due to a large HFCC to ^{31}P; a typical spectrum of **9b** in THF (ca. 8 mM) is shown in Figure 7. The best simulation

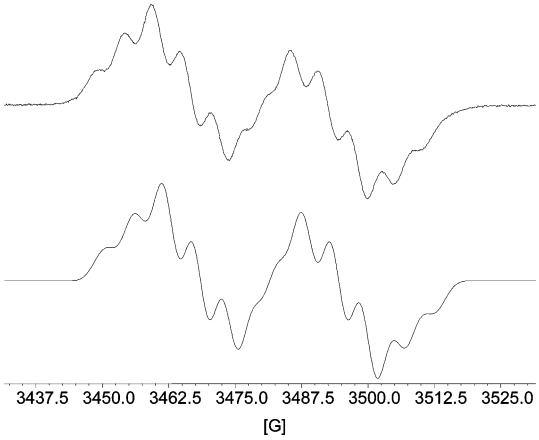

Figure 7. Experimental (top) and simulated (bottom) EPR spectra of **9b** (ca. 8 mM in THF).

of this spectrum is obtained by using a line width of 2.8 G and including HFCCs to one phosphorus atom (26.00 G) and three equivalent nitrogen centers (5.20 G). The distorted or "S-curve" shape of the experimental spectrum is characteristic of a spectrum which contains unresolved hyperfine couplings; the inclusion of a HFCC of 1.05 G to the three equivalent lithium cations reproduces this spectrum in a satisfactory fashion. Due to the broadness of the spectral lines (lw $\approx$ 3.5 G), the HFCCs to the $NSiMe_3$ nitrogen atom and the halogen could not be determined. Though coupling to three equivalent ^{14}N atoms ($I = 1$, 100%) would be expected to result in a doublet of *septets*, overlap at the center of the spectrum combines with line-shape effects to produce the observed pattern.

The C_3 symmetry implied by the EPR spectra is consistent with the cubic structure displayed in the solid state by **3a**,**d** and suggests that these adamantyl-containing radicals are isostructural with the *tert*-butyl analogues **3**. The broad lines observed in the EPR spectra of **9a**,**b** are believed to be due to the steric effects of the bulky adamantyl groups, which causes slow molecular tumbling to a point where the EPR spectra are not entirely isotropic. A similar effect can be seen in the EPR spectrum of **3b** at low temperature,[14] where the cooling of the solvent, THF, restricts the tumbling of **3b**, producing an anisotropic spectrum.

Due to the high computational cost associated with including three NAd groups, DFT calculations have not been carried out for **9a**,**b** to confirm the relative magnitudes of their HFCCs. However, the SOMOs of these radicals are not expected to differ significantly from those of **3a**−**d** and, thus, the model systems **5a**−**d** (Figure 3). In consequence, the HFCCs for the adamantyl derivatives **9a**,**b** are expected to be similar to those observed for their isostructural *tert*-butyl analogues **3a**,**b**, as is indeed the case.

In contrast to the behavior of **3b**,**c**, the EPR spectra of **9a**,**b** are independent of both concentration and temperature and indicate that the C_3 symmetry of these radicals is retained even at extreme dilution. The proposed dissociation pathway of clusters **3b**,**c** is attributed to the coordination of the strong donor solvent THF to the lithium cations, resulting in the cleavage of Li−N bonds and the formation of new Li−O linkages. Consequently, the disruption of the cubic structures

Scheme 2. Synthesis of the Persistent Spirocyclic Radical $\{(THF)_2Li(\mu\text{-}N^tBu)_2P(\mu\text{-}N^tBu)Li(THF)_2\}^\bullet$ (**10a**)

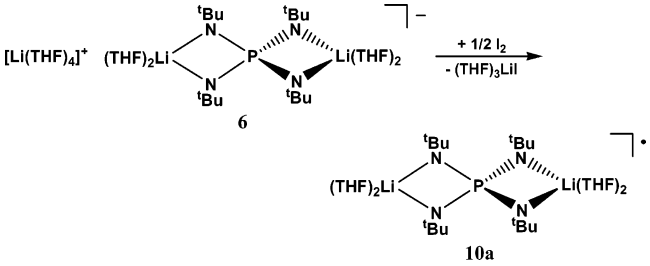

is dependent upon the accessibility of the lithium cations. The fact that this does not occur for **9a**,**b** can be attributed to the additional steric protection which is provided by the adamantyl groups: not only does this aid in the stabilization of these radicals but it also affects the solution behavior of these species by preventing the close approach of additional molecules of THF to the lithium cations so that the cubic frameworks of **9a**,**b** are retained even at extreme dilution.

Formation and EPR Characterization of the Persistent Spirocyclic Radical $\{(THF)_2Li(\mu\text{-}N^tBu)_2P(\mu\text{-}N^tBu)Li(THF)_2\}^\bullet$ (10a). To elucidate the reason for the low stability of the heterobimetallic, spirocyclic radicals $\{Me_2Al[(\mu\text{-}NR)(\mu\text{-}N^tBu)P(\mu\text{-}N^tBu)_2]Li(THF)_2\}^\bullet$ (**4a**, R = $SiMe_3$; **4b**, R = ^{t}Bu),[16] the synthesis of dilithiated analogue **10a** was undertaken according to Scheme 2. Oxidation of the solvent-separated ion pair **6** in THF by addition of 0.5 equiv of iodine or sulfuryl chloride produced a pale blue-green solution which persists for ca. 3 days; attempts to isolate this radical were unsuccessful as it decomposes rapidly in the solid state. The color of the solution is not nearly as intense as that observed in the oxidation of **2b**,**c**, suggesting that radical formation in this instance is either not quantitative or that the radical species is short-lived; this was confirmed by the relatively weak EPR signal produced by the reaction mixture.

The EPR spectra obtained from the iodine- and sulfuryl chloride-oxidized systems were identical, confirming that the same radical is formed in both reactions and that the halogen atom is not bonded to the paramagnetic species. An EPR spectrum of iodine-oxidized **2d** is shown in Figure 8 and displays the doublet of multiplets that is characteristic of the tetraimidophosphate radicals. An excellent simulation of this

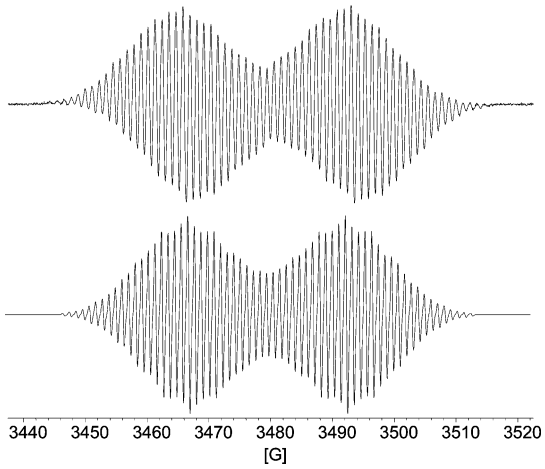

Figure 8. Experimental (top) and simulated (bottom) EPR spectra of **10a**.

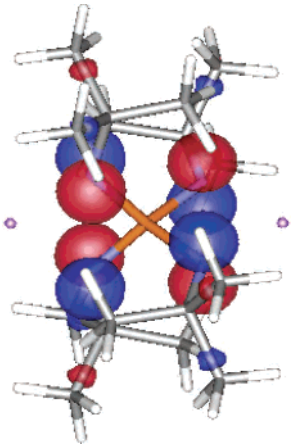

Figure 9. SOMO of **10b** with OMe_2 molecules omitted.

spectrum was obtained by including hyperfine couplings to one phosphorus nucleus ($a^{31}_{P} = 25.60$ G), four equivalent nitrogen atoms ($a^{14}_{N} = 4.25$ G), and two lithium centers ($a^{7}_{Li} = 1.08$ G), which accounts for the observed line spacing. These spectral parameters are consistent with the formation of the spirocyclic radical **10a** in which the unpaired electron is delocalized equally over all four nitrogen atoms. DFT calculations on the geometry-optimized structure of the model system $\{(Me_2O)_2Li(\mu\text{-}N^tBu)_2P(\mu\text{-}N^tBu)Li(OMe_2)_2\}^\bullet$ (**10b**) corroborate a homogeneous spin distribution among the four N^tBu nitrogen atoms; the SOMO of **10b** is shown in Figure 9. The calculated HFCCs for **10b** are in good agreement with those used to create the spectral simulation (Table 4). The EPR spectrum of **10a** is independent of sample concentration, even at extreme dilution, indicating that no dissociation of this radical occurs; this is not surprising since each of the two lithium cations is tightly bound by two highly basic N^tBu groups.

The conspicuous drop in stability from the cubic radicals **3** and **9** to the spirocycle **10a** appears to result from the difference between the geometries of these species. Though the unpaired electron of **10a** is more extensively delocalized (over four N atoms) than in **3** or **9** (over three N atoms), which should render **10a** more stable than its cubic analogues, the reactive nitrogen centers are less sterically protected in the spirocycle **10a** allowing for the more rapid decomposition of the radical to form an intrinsically more stable diamagnetic species, perhaps through dimerization via lithium−nitrogen bond formation. While significantly less stable than **3** or **9**, the spirocycle **10a** is considerably more stable than the heterobimetallic analogues **4a**,**b** which persist for a few hours in solution.[16] This difference can be attributed to the fact that the spin density in **4** is essentially localized on two nitrogen atoms, whereas it is equally distributed over the four nitrogen atoms of **10a**. The trends in stability of the tetraimidophosphate radicals are summarized in Table 5.

Table 5. Stability of Tetraimidophosphate Radicals

Stability	Amount of radical formed	Structure
indefinite in the solid state R = ^{t}Bu, Ad X = Cl, Br, I	quantitative	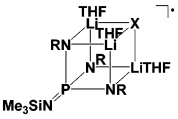
solution only; persists for days	moderate	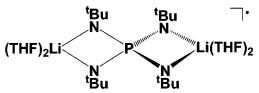
solution only; persists for hours[a]	quantitative	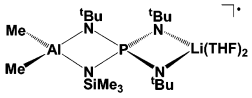
solution only; persists for hours[a]	moderate	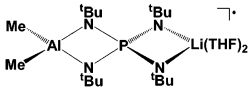

[a] As described in ref 11.

Conclusions

The reaction of $Cl_3PNSiMe_3$ with primary lithium amides is a simple synthetic route to a variety of amino/iminophosphoranes of the type $(RNH)_3PNSiMe_3$ (R = alkyl). Further reaction of such species with ^{n}BuLi under mild conditions produce the unsymmetrical tetraimidophosphates $\{Li_3[P(NR)_3(NSiMe_3)]\}$. Symmetrical tetraimidophosphates $\{[Li_3[P(NR)_4]\}$ can be prepared by the reaction of PCl_5 with excess amine, followed by lithiation with ^{n}BuLi. Oxidation of tetraimidophosphates with iodine, bromine, or sulfuryl chloride produces radicals that are transient when R is a secondary alkyl group but persistent or stable when more bulky R groups are used. For R = Cy, only a transient radical is observed; for R = Ad, the radical retains a cubic structure in solution as steric effects prevent dissociation of the cluster. The symmetrical tetraimidophosphate $\{[Li_3[P(N^tBu)_4]\}$ produces the persistent spirocyclic radical $\{Li_2[P(N^tBu)_4]^\bullet 4THF\}^\bullet$ in solution (Scheme 1); further dissociation to a monocyclic radical is inhibited by the basicity of the N^tBu nitrogen atoms.

Acknowledgment. We thank the University of Calgary and the Natural Sciences and Engineering Research Council of Canada for funding and Helsingin Sanomain 100-vuotissäätiö for a scholarship (H.M.T.), as well as Dr. D. Murphy for attempts to obtain ENDOR spectra of **3**.

Supporting Information Available: Experimental and simulated EPR spectra of **3a**,**c** in hexane and **3c** in THF (limiting spectrum, ca. 2 mM), overlaid experimental and simulated EPR spectra of the aforementioned spectra as well as those in Figures 4−8, and X-ray crystallographic files in CIF format. This material is available free of charge via the Internet at http://pubc.acs.org.

IC051128Q